Peripheral Attention Index: Area-Weighted Distal Polygonal Areas Of Interest

Andrew T. Duchowski[1][0000-0003-1681-7878], Nina A. Gehrer[2][0000-0001-5631-9035], and Jennifer Svaldi[2][0000-0001-9819-4752]

[1] Clemson University, Clemson, SC, USA
duchowski@clemson.edu
https://clemson.edu
[2] University of Tübingen, Tübingen, Germany
[nina.gehrer, jennifer.svaldi]@uni-tuebingen.de
https://uni-tuebingen.de

Abstract. Unary Area-of-Interest (AOI) fixation- or gaze-based selection discards potentially valuable proximal AOIs that fall within the perifoveal or peripheral visual span of attention. This results in abrupt transitions in gaze visualizations with misleading connotations of pinpoint foveal gaze at the exclusion of peripheral influence. We derive a simple, parameter-free Peripheral Attention Index (PAI) that can be used as both an indicator of peripherally influential AOIs and as a simple opacity function that uses the ratio of Object-Gaze Distance (OGD; minimum distance to any AOI vertex) to Centroid-Gaze Distance (OCD) as a geometrically meaningful normalizer. The resulting soft highlighting is fully opaque inside the AOI, decays smoothly outside, and automatically adapts to AOI size and shape. Extensions incorporating AOI area are discussed. The method is computationally straightforward, visually intuitive, and directly compatible with existing eye-tracking pipelines.

Keywords: Eye tracking · Area Of Interest · Attention Mapping.

1 Introduction

Traditional eye-tracking analyses tied to Areas Of Interest (AOIs) assign a binary hit when a gaze point (or fixation) falls inside an AOI and discard all others at that given instant (see Holmqvist et al. [2, Chp.6] and Hooge et al. [3] for excellent reviews of AOI usage). This leads to (1) loss of near-peripheral fixations [14], (2) size-biased dwell-time metrics (if AOI sizes differ), and (3) harsh visual boundaries in gaze visualizations. We extend Wang et al.'s [16] Visual Attention Index (VAI), based on Wang's [15] Object-Gaze Distance (OGD), by considering both polygonal area as well as gaze distance to AOI centroid. These enhancements allow normalization and soft highlighting of peripheral AOIs. The resulting continuous opacity (alpha) channel is based on the ratio of two distances that are simple to compute from standard AOI vertices which allows analyses

(a) gaze point on shin (b) gaze point on waist (c) gaze point on hand

Fig. 1. The Peripheral Attention Index (PAI) identifies polygonal Areas Of Interest (AOIs) that are currently under visual inspection and proximal AOIs that are distal to the gaze point, but potentially influential falling within the peripheral visual span. For visualization, the PAI is used as the transparency channel $\alpha \in [0, 1]$: (a) gaze point falling on shin shows the shin as fully opaque and distal AOIs at increased transparency; (b) gaze point falling on waist; (c) gaze point falling on hand. Notice that in all cases the waist exudes peripheral influence due to its distance and area relative to the gaze point.

that indicate proximal attention to near AOIs (from the one traditionally identified as being viewed) which yields a model of decayed attention to fixated AOIs. We demonstrate the approach as it relates to visualization of viewed body regions in the context of attentional bias measurement that accompanies body dissatisfaction studies in clinical psychology.

Our work builds on Gehrer et al.'s [1] use of Detectron2 [18], a Machine Learning pipeline for identifying body segmentations as viewed by participants looking at themselves in a mirror. Our contributions are three-fold:

1. we polygonize Detectron2's pixelized output by computing the segmentation's alpha shape using Kenneth Bellock's Alpha Shape Toolbox[3],
2. we first refine Wang et al.'s [16] Object-Gaze Distance (OGD) by computing the L2 norm to the closest vertex, not closest AOI pixel—this seems like a small change, but it is important in terms of computational efficiency as there are much fewer vertices than pixels within the AOI regions, and
3. we then further refine the OGD computation by taking account of both the distance from the gaze point to the AOI centroid (yielding the Object-Centroid Distance, or OCD) as well as the AOI's area; both are used to derive a normalized Peripheral Attention Index, or PAI.

We demonstrate the technique by exporting the polygon set to SR Research `.ias` "interest area set" files and interactively simulating gaze with a mouse pointer. As with the OGD and VAI, and in contrast to traditional AOI hit mapping, each fixation is mapped to each AOI continuously throughout the simulation (or

[3] https://alphashape.readthedocs.io/en/latest/

whole trial, depending on use). The value of each AOI's PAI decays smoothly from 1 to 0, representing an AOI hit (1) or < 1 if the gaze point is sufficiently far away but still close enough to register. This is the reverse of the original OGD formulation, but is done purposefully to allow a more aesthetically pleasing visualization using alpha channel transparency.

2 Background

The unary *AOI hit*, evaluated on whether the raw gaze point's or fixation's coordinate is inside the AOI, underlies most raw AOI measures, including those like proportion over time graphs [2, Chp.6]. This is a gaze- or fixation- centric approach that, at the instant of evaluation, selects a single AOI and discards proximal AOIs that may fall within the perifoveal or peripheral visual span of attention.

In his dissertation, Wang [15] challenged conventional eye-tracking analysis based on unary selection of the AOI in which the gaze point landed by rethinking visual attention through the quantification of peripheral vision. He reasoned that to gain a better understanding of task-specific gaze behavior and attention mechanisms, it is imperative to develop adequate gaze measures that can quantify the use of peripheral vision for gaze mapping and attention visualization. Wang proposed the Visual Attention Index (VAI) that, in turn, was based on the definition of the Object-Gaze Distance (OGD). Wang et al. [16] defined the OGD as the minimal L2 norm of each object *area* to the current gaze point. The VAI was then computed as the OGD weighted by the fixation duration.

The VAI is somewhat similar to Rim et al. [7]'s Weighted Sum Durations (WSD). The WSD was a dwell time-like metric, which weighted the duration of fixations by the distance between the fixation and a Point Of Interest (POI). A Gaussian kernel centered at each POI was used to weight the fixation durations, where the kernel's shape and size was kept constant across all POIs. Although perhaps counter-intuitive, the WSD computation is similar to the VAI since larger weights are applied to fixation durations where fixations are closer to the AOI. Hence, the similarity is in the distance-based weighting, as each POI has some influence on the fixation duration.

In both cases, every AOI (or POI) is related to the gaze point by distance and/or duration of the fixation. We are not aware of any other similar approaches to distance-based eye movement analysis, although there are conceptual similarities to the way saliency maps are computed.

We introduce the Peripheral Attention Index (PAI) by extending Wang et al.'s [16] Visual Attention Index by computing the OGD to AOI vertices instead of area, but consider both polygon centroid and polygon area as a normalizing factors (effectively modeling closer and larger AOIs as more influential in the periphery). The PAI is AOI-centric in that at any given instant, multiple AOIs may be currently "hit", but at varying degrees. A snapshot of these AOI hit degrees is similar to what Holmqvist et al. [2] identified as proportion over time

(a) front view (b) side view (c) back view

Fig. 2. Compositing body image onto blank background.

graphs, but the computation is done instantly, in real-time, not via accumulation over time.

3 Body Dissatisfaction & Attentional Bias

Although the Peripheral Attention Index described herein is applicable to general AOI-based eye tracking studies, we demonstrate the approach in the domain of body-related attentional processes that are typically studied in the context of body dissatisfaction and eating disorder pathology in Clinical Psychology [1]. High body dissatisfaction is not only a key symptom but is also a significant risk factor for the development and maintenance of an eating disorder [10].

In line with this, schema-theoretical models assume negative body-related self-schemas as a core factor in eating disorder pathology [17]. Such schemas can include maladaptive acquired beliefs, such as "I am fat.", and are associated with negative affect, dysfunctional eating- and weight-related behaviors (e.g., dieting, self-induced vomiting, excessive sport) and detrimental cognitive biases [17]. These body-related schemas can be activated when confronted with body- or food-related situations or stimuli (e.g., a mirror) and consequently bias attentional, evaluative, and memory processes in favor of schema-consistent information [8,17]. Thus, for example, when viewing one's own body, attention appears to be disproportionately allocated to body parts evaluated as most unattractive while more positively evaluated body parts receive less attention, thereby corroborating the negative view of one's own body and the negative attitude towards it [8,4].

3.1 Assessment of Body-Related Attention Bias

Recording eye movements provides a valuable and comparatively direct measure of overt attention in real time when processing body-related information [4]. Thus, multiple eye-tracking studies have investigated body-related attention biases while viewing images of one's own body or while viewing one's own reflection in a large mirror [4]. Despite varation in methodological approach (e.g., images or mirror, variation in body perspectives, head ommitted or visible), multiple studies have indicated a stronger focus on self-defined negative or unattractive

(a) front view (b) side view (c) back view

Fig. 3. Body pose segmentation from Detectron2's Dense Pose. Note that although the colorized regions appear polygonal, they are internally represented as color-labeled pixels only, lacking polygon bounding edges.

relative to attractive regions of one's own body in association with eating disorder diagnoses [12,6,13] as well as body dissatisfaction [1,9].

Unfortunately, the analysis of eye-tracking data, in particular, has so far been very time-consuming and may be prone to subjective misjudgments or biases, as, for example, the AOIs (in this case the different body regions) typically have to be defined manually or the data analysis is based on a frame-based subjective rating of which body part was looked at [4,5,11].

To facilitate and optimize these processes, an automated analysis routine for defining AOIs should be used to increase the efficiency and objectivity of data analysis [1]. Given that this previous validation study utilizing mobile eye-tracking data from a standardized mirror setting suggested that body perspective (front vs. side view) may affect the accuracy of the approach, we decided to use still images of one's own body including three perspectives (i.e., front, side, and back view) as shown in Fig. 2. To increase ecological validity of the viewed images, the chroma-keyed (colloquially called green-screen) composition of the body can be placed on a background resembling, e.g., gym, bathroom, bedroom, etc.

To automate the gaze analytics pipeline as much as possible, the pipeline is split into the following steps:

1. identify and label body parts, e.g., via image segmentation;
2. further segment those parts that require it (e.g., torso into waist, chest, etc.);
3. convert body part regions into polygonal AOIs;
4. output polygons into a known file format;
5. compute gaze- or fixation-based metrics relative to AOIs, e.g., via the PAI.

4 Definition and Implementation of the PAI

Wang's computation of the OGD was somewhat loosely defined, as the term *area* connoted computation of the *minimum* L2 norm (Euclidean distance) from the gaze point to the *pixel set* of the AOI. This was done because the output of the

(a) front view (b) side view (c) back view

Fig. 4. Result of shape alpha polygonization. Colorized regions are now represented by polygon vertices and edges enclosing the interior region. Note that alpha shape polygonization can sometimes produce erroneous polygonal boundaries, e.g., when body regions are confused with regions in the background such as chairs (when body pose estimation and polygonization is performed on composite image, for example). In this instance, polygonization is done on the extracted foreground alone, but body pose estimations fails partially on the side image, (b).

Machine Learning model used returns pixels that are labeled (or colored, in the algorithmic sense, if you prefer) as belonging to a specific member of the AOI set (e.g., pixels colored to indicate pixel membership in the upper arm region, lower leg, etc.). Thus, each AOI is basically a set of pixels, and the minimum L2 norm is simply the Euclidean distance from the gaze point to the closest pixel in the set. More formally, $\mathrm{OGD} = \min_i \|[\mathbf{G} - \mathbf{p}_i\|_2$ where $\mathbf{G}$ is the gaze point (x, y) and $\mathbf{p}_i = (x_i, y_i)$ is the i^{th} pixel, $i \in 1, \ldots n$ of the given AOI.

The use of Detectron2, a body pose estimator, produces very similar region-labeled pixel sets as it also uses a similar Machine Learning model to perform body pose segmentation, see Fig. 3. However, to facilitate both interoperability with SR Research's Data Viewer, as well as the PAI computation, we first polygonize the pixel regions by computing *alpha shapes* for each region. Computing the alpha shape is similar to the computation of a convex hull. In fact, the alpha shape depends on a real number a such that if $a = 0$ a convex hull is produced. We use $a = 0.1$ which tends to "hug" the pixel shape more tightly than the convex hull. This is important for body shape regions although the computation is somewhat prone to error if the body pose is not ideally perpendicular to the camera (e.g., standing sideways), see Fig. 4.

Following computation of an alpha shape for each AOI, each AOI is now defined by polygonal vertices instead of the pixels within. We can now redefine the OGD to be computed as $\mathrm{OGD} = \min_i \|\mathbf{G} - \mathbf{v}_i\|_2$ where $\mathbf{G} = (x, y)$ is the current gaze point, as before, and $\mathbf{v}_i = (x_i, y_i)$ is now the i^{th} AOI polygon vertex. This is a subtle but important difference since the expectation is that there will be much fewer vertices than pixels, and so the OGD computation will be much more efficient. Note, however, that polygonization can lead to erroneous boundaries, especially if the body pose estimation is performed on the composite images instead of the greenscreen extracted foreground body images (where background noise is eliminated or at least reduced).

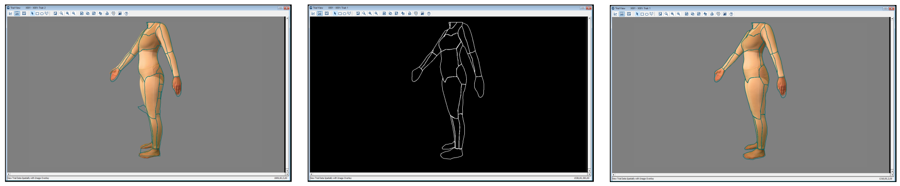

(a) Data Viewer import (b) polygon view (c) following manual fix

Fig. 5. Polygonal correction in SR Research Data Viewer.

Because polygonal data is defined by a list of vertices (and implicit edges), this data can now be exported as SR Research `.ias` "interest area set" files which can then be read in by SR's Data Viewer and interactively manipulated (e.g., to shift misaligned polygons and/or removal of errant vertices). Such manipulation is shown in Fig. 5.

Given that each AOI is now represented as a polygon, two important properties fall out through alpha shape computation: (1) polygon area via the Shoelace (Gauss's area) $O(n)$ efficient computation for n vertices,

$$A = \frac{1}{2}\left|\sum_{i=1}^{n}(x_i y_{i+1} - x_{i+1} y_i)\right|$$

where (x_i, y_i) are the vertex coordinates and $(x_{n+1}, y_{n+1}) = (x_1, y_1)$, and (2) polygon centroid $(\bar{x}, \bar{y})$ computation:

$$\bar{x} = \frac{1}{6A}\sum_{i=1}^{n}(x_i + x_{i+1})(x_i y_{i+1} - x_{i+1} y_i)$$
$$\bar{y} = \frac{1}{6A}\sum_{i=1}^{n}(y_i + y_{i+1})(x_i y_{i+1} - x_{i+1} y_i)$$

where $(x_{n+1}, y_{n+1}) = (x_1, y_1)$, the polygon is closed, as before. Denoting the polygon centroid as $\mathbf{C} = (\bar{x}, \bar{y})$, we can now compute the Centroid-Gaze Distance (CGD): $\|\mathbf{G}-\mathbf{C}\|_2$. This now allows us to compute the Peripheral Attention Index as a proposed alpha channel opacity:

$$\alpha = 1 - \sqrt{\frac{\mathrm{OGD}}{\mathrm{CGD}}}. \tag{1}$$

When $\mathbf{G}$ lies inside or on the AOI boundary, OGD $= 0 \rightarrow \alpha = 1$ (fully opaque). As $\mathbf{G}$ moves away, α decays smoothly to 0. The square-root yields a concave decay profile similar to Gaussian attention fall-off models while remaining monotonic and computationally negligible. A minimal Python implementation is given in Listing 1.1.

```
import numpy as np

def compute_ogd(x_g, y_g, aoi):
    verts = np.array(aoi)
    dists = np.sqrt((verts[:,0]-x_g)**2 + (verts[:,1]-y_g)**2)
    return dists.min()

def compute_cgd(x_g, y_g, aoi):
    verts = np.array(aoi)
    centroid = verts.mean(axis=0)
    return np.hypot(x_g - centroid[0], y_g - centroid[1])

def soft_alpha(x_g, y_g, aoi, area_weight=True, A_ref=50000):
    ogd = compute_ogd(x_g, y_g, aoi)
    cgd = compute_cgd(x_g, y_g, aoi)
    if cgd == 0: return 1.0
    ratio = np.sqrt(ogd / cgd)
    if area_weight:
        A = 0.5 * np.abs(np.dot(aoi[:,0], np.roll(aoi[:,1],1)) -
                         np.dot(aoi[:,1], np.roll(aoi[:,0],1)))
        ratio *= min(1.0, A / A_ref)
    return np.clip(1.0 - ratio, 0.0, 1.0)
```

Listing. 1.1. PAI (soft alpha) implementation where `A_ref` is the max polygonal area, which can be pre-computed with a finite AOI set.

4.1 Area-Weighted Extension

Larger AOIs naturally capture more peripheral attention. Or, stated another way, the probability of attention landing in a given AOI is proportional to its size. To prevent small objects from vanishing too quickly, we optionally weight by relative area A (computed via the Shoelace formula):

$$\alpha_A = 1 - \sqrt{\frac{\mathrm{OGD}}{\mathrm{CGD}}} \cdot \min\left(1, \frac{A}{A_{\mathrm{ref}}}\right) \tag{2}$$

where A_{ref} is a reference area (e.g., maximum AOI area in the stimulus). Note that A_{ref} can be pre-computed in time linear proportional to the number of AOIs. The choice of maximum or median is optional.

4.2 Theoretical Properties

Theorem 1. *For any simple polygon with $n \geq 3$ vertices and centroid $\mathbf{C}$ strictly interior to the polygon, OGD $\leq$ CGD holds for all gaze points $\mathbf{G} \in \mathbb{R}^2$, with equality only in degenerate cases.*

Proof. Let $v^* = \arg\min_i \|\mathbf{G} - v_i\|_2$ so $\text{OGD} = \|\mathbf{G} - v^*\|_2$. The centroid is $\mathbf{C} = \frac{1}{n}\sum_{i=1}^{n} v_i$. Then

$$\begin{aligned}
\text{CGD} &= \left\| \mathbf{G} - \frac{1}{n}\sum_{i=1}^{n} v_i \right\|_2 = \left\| \frac{1}{n}\sum_{i=1}^{n} (\mathbf{G} - v_i) \right\|_2 \\
&\geq \frac{1}{n}\sum_{i=1}^{n} \|\mathbf{G} - v_i\|_2 \quad \text{(triangle inequality)} \\
&\geq \frac{1}{n}\left(\|\mathbf{G} - v^*\|_2 + (n-1)\cdot\|\mathbf{G} - v^*\|_2\right) \\
&= \|\mathbf{G} - v^*\|_2 = \text{OGD}.
\end{aligned}$$

Equality holds only if all vectors $\mathbf{G} - v_i$ are parallel and of equal length (degenerate polygon).

Corollary: $\frac{\text{OGD}}{\text{CGD}} \in [0, 1]\ \forall \mathbf{G}$, making (1) a valid, parameter-free opacity.

5 Discussion and Related Work

Equation (1) shares the spirit of distance-weighted AOI metrics [7,16] that extend unary membership with probabilistic or soft assignments. Unlike Rim et al.'s [7] Gaussian kernels with manually tuned σ, our approach is data-driven: the CGD serves as an intrinsic scale parameter proportional to the AOI's effective radius. The resulting visualizations eliminate abrupt boundaries while preserving full opacity inside AOIs—a property valued in both static attention maps and real-time gaze-overlay visualizations.

6 Conclusion

We presented a theoretically grounded, parameter-free opacity function for soft AOI highlighting that adapts automatically to AOI geometry and size. Although one of its primary uses is visualization of the potential influence of AOIs that are proximal to the one currently attended to via the gaze point (or fixation), the numerical quantification of this influence is a novel approach to the consideration of AOI during analysis of eye movement during the time course of viewing the given stimulus. Since the PAI can be non-zero for multiple AOIs at any given instant, AOI-based analysis is thus radically changed from the unary *AOI hit* paradigm conventionally used in eye movement research. Note the PAI as implemented acts as an "instantaneous" metric, when attention is dynamic, it can also be used over time, if buffered. In this instance, the PAI will produce similar *decaying* heatmap-like visualization of active and decaying attention.

Acknowledgements SuperGrok [19], an AI model developed by xAI, was used to develop some of the computational methods and explanations and to generate

initial code, i.e., the method was conceptualized by the authors, SuperGrok mainly provided coding support. Everything generated was revised and refined to ensure accuracy and alignment with research objectives.

References

1. Gehrer, N.A., Svaldi, J., Duchowski, A.: Assessment of body-related attention processes via mobile eye tracking: A pilot study to validate an automated analysis pipeline. In: Proceedings of the 2024 Symposium on Eye Tracking Research and Applications. ETRA '24, Association for Computing Machinery, New York, NY (2024). https://doi.org/10.1145/3649902.3653354, https://doi.org/10.1145/3649902.3653354 2, 4, 5
2. Holmqvist, K., Nyström, M., Andersson, R., Dewhurst, R., Jarodzka, H., Van de Weijer, J.: Eye Tracking: A Comprehensive Guide to Methods and Measures. Oxford University Press (2011) 1, 3
3. Hooge, I.T.C., Nyström, M., Niehorster, D.C., Andersson, R., Foulsham, T., Nuthmann, A., Hessels, R.S.: The Fundamentals of Eye Tracking Part 6: Working with Areas Of Interest. Journal of Behavior Research Methods **58**(65), 1–29 (2026). https://doi.org/10.3758/s13428-025-02937-3 1
4. Kerr-Gaffney, J., Harrison, A., Tchanturia, K.: Eye-tracking research in eating disorders: A systematic review. International Journal of Eating Disorders **52**(1), 3–27 (2019) 4, 5
5. Krohmer, K., Derntl, B., Svaldi, J.: Hormones Matter? Association of the Menstrual Cycle With Selective Attention for Liked and Disliked Body Parts. Frontiers in Psychology **10**, 851 (2019). https://doi.org/10.3389/fpsyg.2019.00851 5
6. Krohmer, K., Naumann, E., Tuschen-Caffier, B., Svaldi, J.: Taking a closer look at body processing in binge eating disorder–Influence of BMI and eating pathology. Behaviour Research and Therapy **156**, 104106 (2022) 5
7. Rim, N.W., Choe, K.W., Scrivner, C., Berman, M.G.: Introducing Point-of-Interest as an alternative to Area-of-Interest for fixation duration analysis. PLOS ONE **16**(5), 1–18 (05 2021). https://doi.org/10.1371/journal.pone.0250170, https://doi.org/10.1371/journal.pone.0250170 3, 9
8. Rodgers, R.F., DuBois, R.H.: Cognitive biases to appearance-related stimuli in body dissatisfaction: A systematic review. Clinical Psychology Review **46**, 1–11 (2016). https://doi.org/10.1016/j.cpr.2016.04.006 4
9. Roefs, A., Jansen, A., Moresi, S., Willems, P., van Grootel, S., van der Borgh, A.: Looking good. BMI, attractiveness bias and visual attention. Appetite **51**(3), 552–555 (2008). https://doi.org/10.1016/j.appet.2008.04.008 5
10. Stice, E.: Interactive and Mediational Etiologic Models of Eating Disorder Onset: Evidence from Prospective Studies. Annual Review of Clinical Psychology **12**, 359–381 (2016). https://doi.org/10.1146/annurev-clinpsy-021815-093317 4
11. Svaldi, J., Bender, C., Caffier, D., Ivanova, V., Mies, N., Fleischhaker, C., Tuschen-Caffier, B.: Negative Mood Increases Selective Attention to Negatively Valenced Body Parts in Female Adolescents with Anorexia Nervosa. PLoS ONE **11**(4), e0154462 (2016). https://doi.org/10.1371/journal.pone.0154462 5
12. Svaldi, J., Caffier, D., Tuschen-Caffier, B.: Attention to Ugly Body Parts Is Increased in Women with Binge Eating Disorder. Psychotherapy and Psychosomatics **80**(3), 186–188 (2011). https://doi.org/10.1159/000317538 5

13. Tuschen-Caffier, B., Bender, C., Caffier, D., Klenner, K., Braks, K., Svaldi, J.: Selective visual attention during mirror exposure in anorexia and bulimia nervosa. PLoS ONE **10**(12), e0145886 (2015) 5
14. Wang, F.S., Wolf, J., Farshad, M., Meboldt, M., Lohmeyer, Q.: Object-Gaze Distance: Quantifying Near-Peripheral Gaze Behavior in Real-World Applications. Journal of Eye Movement Research **19**(14) (May 2021). https://doi.org/10.16910/jemr.14.1.5 1
15. Wang, F.S.: Algorithmic Gaze Measure Development for Application in Real-World Scenarios. Ph.D. thesis, ETH Zürich, Zürich, Switzerland (2023). https://doi.org/10.3929/ethz-b-000616462, diss. ETH No. 29299 1, 3
16. Wang, F.S., Lohmeyer, Q., Duchowski, A., Meboldt, M.: Gaze is more than just a point: Rethinking visual attention analysis using peripheral vision-based gaze mapping. In: Proceedings of the 2023 Symposium on Eye Tracking Research and Applications. ETRA '23, Association for Computing Machinery, New York, NY (2023). https://doi.org/10.1145/3588015.3589840 1, 2, 3, 9
17. Williamson, D.A., White, M.A., York-Crowe, E., Stewart, T.M.: Cognitive-behavioral theories of eating disorders. Behavior Modification **28**(6), 711–738 (2004). https://doi.org/10.1177/0145445503259853 4
18. Wu, Y., Kirillov, A., Massa, F., Lo, W.Y., Girshick, R.: Detectron2. online (2019), https://github.com/facebookresearch/detectron2 2
19. xAI: Grok: An Artificial Intelligence Model for Scientific and Technical Assistance (2025), https://x.ai/grok, Version accessed: August 2025 9